Compact → Extended Helix Transitions of Polyalanine in Vacuo

Anne E. Counterman[†] and David E. Clemmer*

Department of Chemistry, Indiana University, Bloomington, Indiana 47405

Received: June 5, 2002; In Final Form: November 26, 2002

The relative stabilities of conformations of $[Ala_n + 3H]^{3+}$ peptides (where $n = 27-39$) have been examined in the gas phase using ion mobility/time-of-flight techniques. At room temperature, two series of conformations that do not interconvert during the $10-40$-ms experimental time scales are observed: extended helical structures and more compact geometries assigned as hinged helix-coils (Counterman, A. E.; Clemmer, D. E. *J. Am. Chem. Soc.*, **2001**, *123*, 1490). At elevated temperatures, a single structural transition is observed; the more compact state unfolds and adopts extended helical structures for all sizes. Relative activation energies for the compact → extended helix transitions increase linearly by ∼1 kcal·mol^{-1}·residue^{-1} over the $n = 27-39$ size range. Mechanisms that consider important steps in the helix-coil → helix transition are discussed. We propose that release of the hinge might be a difficult step in this transition that is instigated by intramolecular reorganization of protons.

Introduction

Understanding stabilities of helices, sheets, and folds and the transitions between these elements of structure is central to the protein-folding problem.[1,2] The stabilities of helices have been examined in detail for sequences of alanine-rich peptides in a range of environments.[3−6] Although detailed information for these systems is available, the issue of whether the alanine residue is intrinsically helix-stabilizing still attracts significant experimental attention.[7] The recent development of electrospray ionization (ESI)[8] for mass spectrometry (MS) allows intrinsic structural properties of peptide chains to be examined in vacuo.[9] Ion mobility studies[10] and molecular dynamics simulations[11] indicate that singly protonated polyalanine peptides ($[Ala_n + H]^+$, where $n = 3-20$) exist as compact globules. In these systems, electronegative carbonyl groups along the polypeptide backbone wrap around the protonated amino group to solvate the charge. Incorporation of a single basic Lys residue at the C-terminal end of these peptides (i.e., $[Ala_n\text{-Lys} + H]^+$, $n = 7-19$) leads to helices.[12] When the peptide is protonated at a C-terminal Lys residue, the charge can be capped by interactions with carbonyl groups that extend from the end of the helix.

Recently, our laboratory examined a series of larger multiply charged peptides, $[Ala_n + zH]^{z+}$ ($n = 5-49$ and $z = 1-4$).[13] In this system, $[Ala_n + 3H]^{3+}$ ($n = 24-41$) ions exhibit two families of conformations that are stable at room temperature over the millisecond experimental time scales. From molecular modeling studies, it appears that, when net charge is distributed on the C-terminal side of the peptide [i.e., $(\Sigma i)/3 > n/2$, where i denotes the residues at which charges are located and n is the number of residues in the peptide], the polymer adopts an extended conformation and exhibits significant α-helical character. Simulations of the extended helical state show that >90% of the residues participate in $i \rightarrow i + 4$ hydrogen bonding; deviations from α-helical character occur primarily at the N-terminus or adjacent to charge sites. Alternatively, if the net position of charge is distributed on the N-terminal side [i.e.,

$(\Sigma i)/3 < n/2$], the peptide favors more compact states. The combined experimental and molecular modeling results for these peptides indicate that the N-terminal portion of the chain folds back (in a largely random fashion), producing a range of conformers that we describe as hinged helix-coils. Model compact conformers that are in close agreement with experiment have structures in which the polymer chain folds roughly in half, with a proton at the N-terminus stabilizing a C-terminal region of helix. The remaining N-terminal side of the polymer appears to be closely associated with the helix, but molecular modeling results suggest that many variations of the coil-helix interaction are possible. Figure 1 shows model geometries that are representative of the two structural types. In this representation, charges located at the $i = 12$, 24, and 36 positions favor extended helical structures; the more compact conformer was generated by placing protons at the $i = 1$, 8 and 16 positions. As described previously,[13] many other N-terminal side (e.g., 1, 6, 12; 1, 9, 10; and 1, 16, 30) and C-terminal side (e.g., 1, 19, 36; 10, 21, 36; and 11, 27, 36) charge site assignments result in similar low-energy structures.

In this paper, we examine the relative stabilities of these states. At elevated source temperatures, we find evidence for a single type of structural transition. Compact conformers appear to convert directly into extended helices for all sizes; no intermediates associated with this transition are observed. Relative activation energies for the conversion of compact forms to extended helical states are reported. Although theory has examined the stabilities of structural elements in biopolymers in vacuo for many years,[14] few experimental studies to date have addressed the energetics of structural transitions in the gas phase.[15,16] The present data are the first measures of transitions for a particular conformational type in vacuo as a function of polymer length. Possible mechanisms for transitions leading to helix formation are considered.

Experimental Section

Nested Drift (Flight) Time Measurements. Detailed descriptions of ion-mobility techniques[17,18] and methods for generating structural information[9d,19,20] have been given previously. The data presented below were recorded using an ion

---

* To whom correspondence should be addressed.

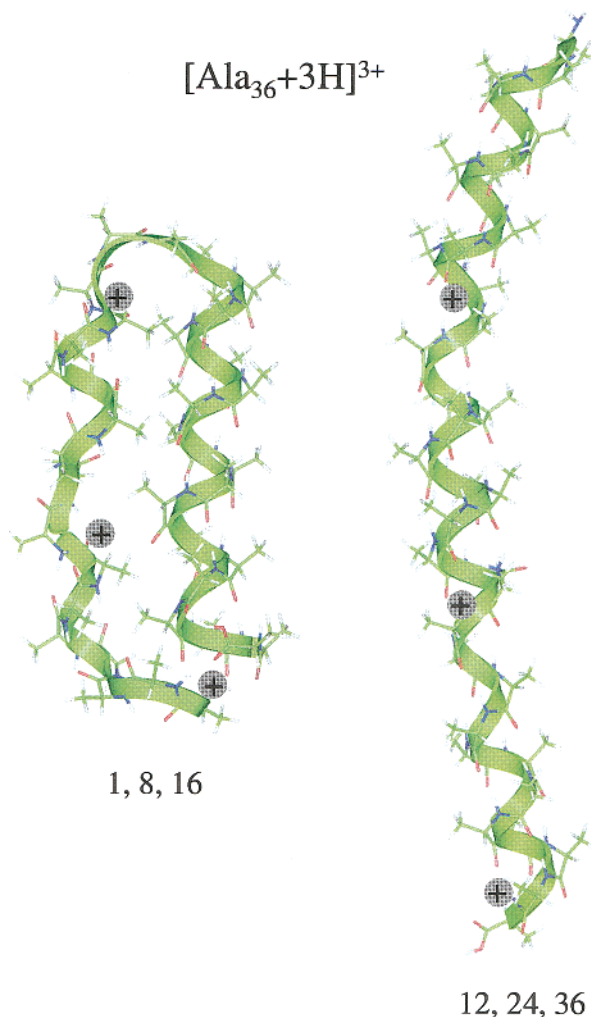† Current address: Department of Chemistry, Pennsylvania University, University Park, PA 16802.

$[Ala_{36}+3H]^{3+}$

1, 8, 16

12, 24, 36

Figure 1. Representative hinged helix-coil and extended helical conformations proposed for $[Ala_n + 3H]^{3+}$ ions. Protonation sites are indicated by shaded spheres and + symbols. The particular structures shown here are from molecular dynamics simulations of $[Ala_{36} + 3H]^{3+}$ in the 1, 8, 16 and 12, 24, 36 charge configurations [charge sites along the backbone are numbered such that the N-terminus is 1 and the amide of the C-terminal residue is *n* (in this case, 36)]. See ref 13 for computational details.

mobility/time-of-flight apparatus.[21] A brief overview of the experimental sequence is as follows. Solutions of polyalanine peptides [Sigma, nominal 1000−5000 g/mol molecular weight range; $(5.6 \times 10^{-5})-(2.8 \times 10^{-4})$ M in a 49:49:2 water/acetonitrile/acetic acid mixture] were electrosprayed[8] into a heated capillary source[22] similar to those described in the literature.[23,24] The design of the source allows the capillary length to be varied. After exiting the capillary, ions are cooled to 298 K by collisions with the drift gas and guided to the drift region through a series of closely spaced (0.3 cm) electrostatic lenses. Short pulses (300 μs in duration) of ions are introduced into the drift region, where they drift through the helium buffer gas (~180 Torr) under the influence of a uniform electric field (137.4 V·cm⁻¹). Under the low-field conditions employed, the mobilities of ions through the helium buffer gas depend on the ion geometries and charge states. For a given charge state, compact ions (with relatively small collision cross sections) have higher mobilities than more elongated ions.[25] As ions exit the drift tube, they are pulsed into a reflectron geometry time-of-flight mass spectrometer. The flight time measurement is synchronized with the initial injection of ions into the drift region. Because drift times through the helium buffer gas are

much longer (milliseconds) than flight times in the mass spectrometer (microseconds), hundreds of flight time distributions can be acquired for each pulse of ions that is introduced into the drift tube. Thus, mobilities and *m/z* values for all ions are obtained simultaneously. We refer to the two-dimensional datasets as nested drift (flight) time distributions.[21] Complete descriptions of ion mobility/mass spectrometry methods, including data acquisition systems, are provided elsewhere.[21]

Temperature-Dependent Measurements. The temperature-dependent source is constructed in a modular fashion, allowing some variability in the capillary length. The majority of experiments presented here were conducted using a 19.0-cm-long, 0.13-cm-diameter stainless steel capillary. In a smaller number of experiments, capillary lengths were varied by up to a factor of 3. Relative thermochemical values from all three source lengths agree within the experimental uncertainty (see below). The source is designed such that the capillary inserts into an aluminum block equipped with six equally spaced cartridge heaters. During experiments, the temperature of the external source was measured using a chromel/alumel thermocouple (i.e., type K) connected to a digital panel meter (Omega International, Stamford, CT). In a separate experiment, the external source temperatures were calibrated with respect to the temperature of the gas in the center of the capillary. We estimate that the calibrated temperatures should reflect the temperatures of the ions to within ±8 °C (at the highest temperatures measured). All of the measurements reported here for elevated source capillary temperatures were recorded in consecutive experiments to minimize differences in experimental parameters that might influence the relative abundances of ion conformers. Although we have attempted to create a highly uniform temperature across the capillary, it is clear that this environment is somewhat ill-defined. For example, some collisions with solvent in this region could occur and influence our measurements. Thus, all thermochemical values are reported as relative values. This is essentially equivalent to the approach taken previously by Smith and co-workers.[28]

Molecular Modeling Simulations of Compact → Helix Transition. To provide insight into the important steps of the compact → helix transition, molecular dynamics simulations were performed. The simulations were carried out at 300 and 400 K for at least 0.25 ns (some simulations were run for up to 2 ns) using the extensible systematic force field (ESFF) and a dielectric of 1.0. This procedure is analogous to the approach we described previously.[13] The $[Ala_n + 3H]^{3+}$ system is, by nature, complex. There are numerous proton configurations and starting geometries that would be reasonable starting points for modeling the compact → extended helix transition. We have reduced the calculations to a manageable size by choosing a model case that appears to capture some general features of the compact → extended helix transition. For the starting geometries, we chose hinged helix-coil conformers (such as that shown in Figure 1) generated from our previous 300 K molecular dynamics simulations of several different charge site assignments of $[Ala_{36} + 3H]^{3+}$ (e.g., 1, 8, 16; 1, 6, 12; 1, 9, 10; and 1, 16, 30). The hinged helix-coil is proposed as the compact $[Ala_n + 3H]^{3+}$ state for reasons that were explained previously[13] and on the basis of additional supporting evidence outlined below. All protons were assumed to be located on amide backbone groups as previously noted.[13]

Results

Drift (Flight) Time Distributions. Figure 2 shows a small region of the nested drift (flight) time distributions recorded

Compact → Extended Helix Transitions of Polyalanine

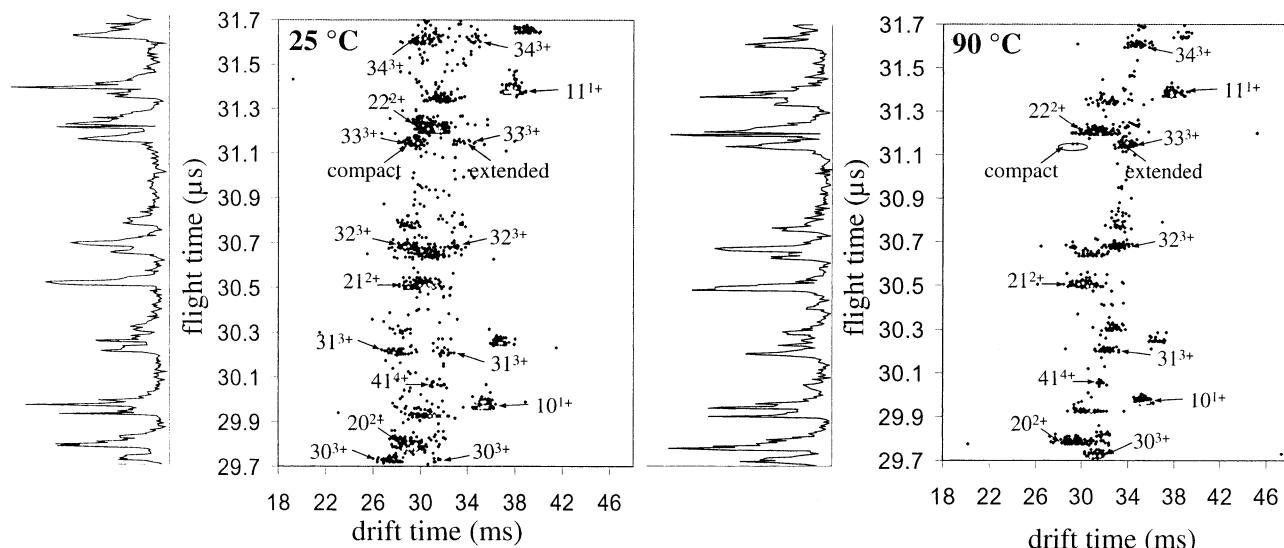*J. Phys. Chem. B, Vol. 107, No. 9, 2003* **2113**

Figure 2. Drift (flight) time distributions recorded for a mixture of polyalanine ions at source capillary temperatures of (left) 25 °C and (right) 90 °C. Both datasets were recorded at an electric field strength of 137.4 V·cm⁻¹. The drift time axes are normalized to a helium pressure of 200.00 Torr. Each two-dimensional dataset is plotted using an intensity cutoff of 2; data points below this value are not represented. To the left of each distribution is the corresponding time-of-flight mass spectrum obtained by integrating the ion signal at each flight time over all drift times. Peak assignments are labeled as n^{z+} (where n is the number of alanine residues and z is the ion charge state). Unlabeled peaks correspond to $[\mathrm{Ala}_n + z\mathrm{H} + 14]^{z+}$ ions. In each spectrum, the location of the compact and extended helical states for $[\mathrm{Ala}_{33} + 3\mathrm{H}]^{3+}$ are indicated; an oval is used to delineate the location of the low-intensity compact state in the 90 °C data.
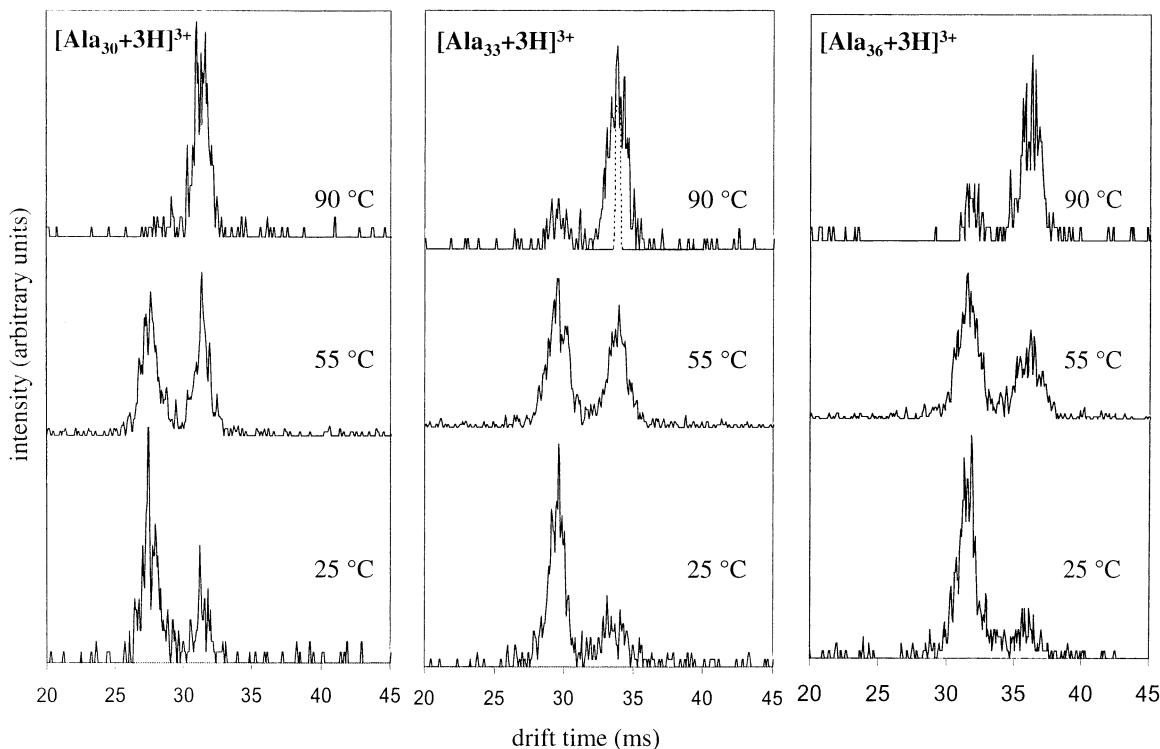

Figure 3. Ion mobility distributions obtained for $[\mathrm{Ala}_{30} + 3\mathrm{H}]^{3+}$ (left), $[\mathrm{Ala}_{33} + 3\mathrm{H}]^{3+}$ (middle), and $[\mathrm{Ala}_{36} + 3\mathrm{H}]^{3+}$ (right) by taking slices of the drift (flight) time datasets recorded for a polyalanine mixture at source capillary temperatures of 25, 55, and 90 °C. All distributions are normalized to a buffer gas pressure of 200.00 Torr and an electric field strength of 137.4 V·cm⁻¹. The dotted line superimposed on the $[\mathrm{Ala}_{33} + 3\mathrm{H}]^{3+}$ (90 °C) distribution indicates the expected distribution for transport of a single conformer type through the drift tube.

for a mixture of polyalanine ions at calibrated source temperatures of 25 and 90 °C. Over the entire range of data recorded for both distributions, we observe $[\mathrm{Ala}_n + z\mathrm{H}]^{z+}$ ions, where $n = 5-49$ and $z = 1-4$. The distributions of sizes and charge states are consistent with our previous results.[13]

Over the $n = 24-40$ size range, $[\mathrm{Ala}_n + 3\mathrm{H}]^{3+}$ ions show two resolved peaks across the ion mobility dimension. Cross sections derived from these data[17] are consistent with values that we have reported[13] and are assigned as compact (hinged

helix-coil, or HHC) conformers and extended helical (EH) conformers.[13] It is important to consider how the distribution of charge states and sizes is influenced by the source temperature. An examination of mass spectra from each drift (flight) time distribution (obtained by integrating the ion intensities at each flight time over all drift times, Figure 2) shows that, over the 25−90 °C range of calibrated source temperatures, no reproducible variations can be observed between mass spectra recorded at different temperatures. This indicates that the relative
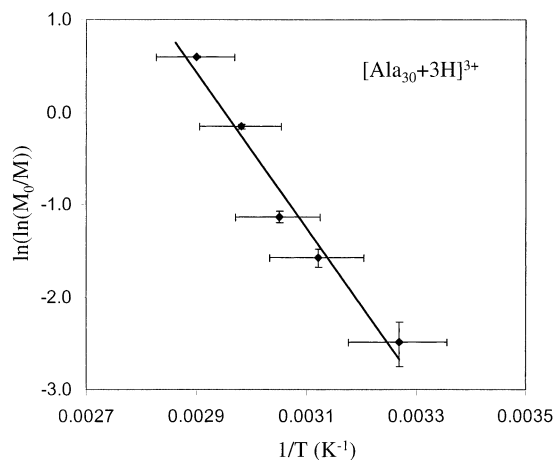
Figure 4. Plot of $\ln(\ln([M_c]_0/[M_c]_1))$ against T^{-1} for the $[Ala_{30} + 3H]^{3+}$ compact (hinged helix-coil) → extended helix transition. See text and eq 3 for details. Estimated uncertainties of ±8 °C in temperature and 2% in integrated ion abundance are shown.
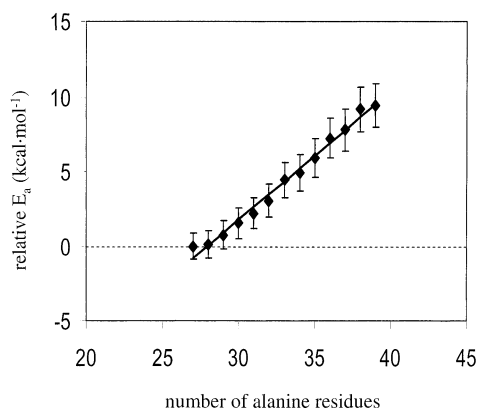

Figure 5. Relative activation energies (kcal·mol^{-1}) obtained for the compact → extended helical transition for $[Ala_n + 3H]^{3+}$ where $n = 27-39$. Relative values are obtained by taking the activation energy derived for $[Ala_{27} + 3H]^{3+}$ to be 0 (see text). Uncertainties corresponding to one standard deviation about the mean are derived for each polymer size from the linear regression analysis used to obtain the slope of eq 3.

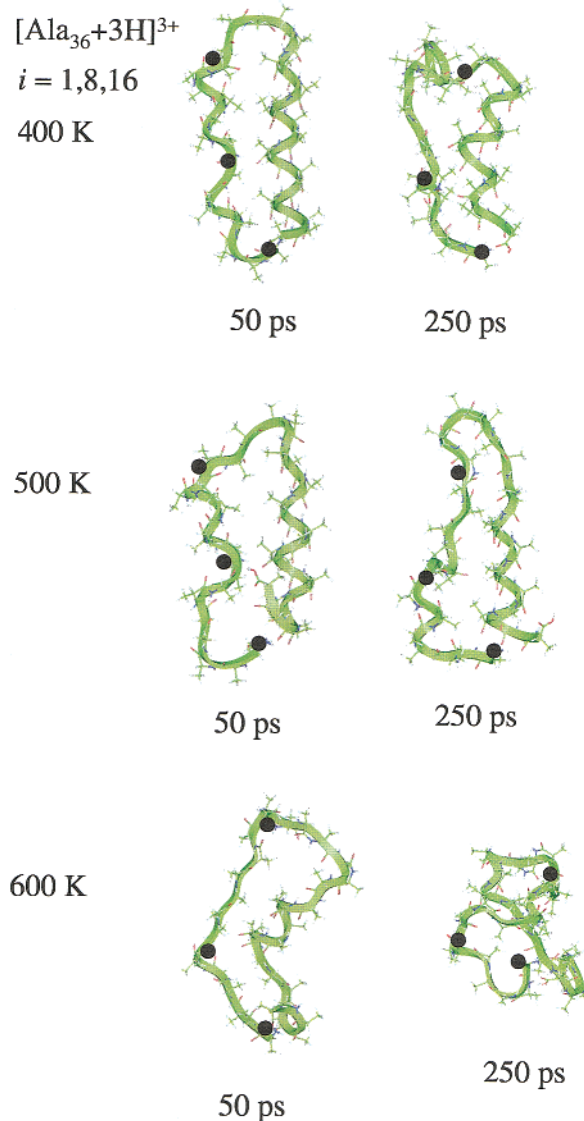**Figure 6.** Model $[Ala_{36} + 3H]^{3+}$ conformers obtained by 50 and 250 ps from 400 and 500 K molecular dynamics simulations started from an HHC geometry having an $i = 1, 8, 16$ charge site assignment (shown in Figure 1).

abundances of different polymer sizes and the distributions of charge states are not influenced by temperature. It further suggests that ion−molecule reactions in the source do not substantially affect these results.

Although the mass spectra recorded at different temperatures are indistinguishable, significant changes in the drift time distributions are found. For example, the relative abundances of the two $[Ala_n + 3H]^{3+}$ conformers change substantially. The two-dimensional plot shows that, at the 90 °C source temperature, the abundance of compact conformers is much smaller than it is at 25 °C. Figure 3 shows representative drift time distributions for the $[Ala_{30} + 3H]^{3+}$, $[Ala_{33} + 3H]^{3+}$, and $[Ala_{36} + 3H]^{3+}$ ions, obtained by taking narrow slices across two-dimensional datasets recorded at calibrated source temperatures of 25, 55, and 90 °C. At 25 °C, compact conformers comprise 70, 73, and 84% of the population for $n = 30, 33$, and 36, respectively, far greater than 30, 27, and 16% abundances for the extended helical conformers of these respective ions. At 55 °C, the percentages of compact conformers decrease to 53, 57, and 61%, respectively, and there is a corresponding increase in the abundances of helical conformers. At 90 °C, helical conformers dominate the distributions, comprising ~90, 84, and 80% for $n = 30, 33$, and 36, respectively. All other $[Ala_n + 3H]^{3+}$ polymer sizes show that the extended helices are favored

at elevated source temperatures. Data obtained using other capillary lengths exhibit analogous behavior.

Several conclusions regarding the relationship of the compact and extended states can be made. First, the increase in the abundance of the elongated conformer corresponds directly to the decrease in the more compact states. Thus, the compact → extended helix transition appears to be direct, with no isolable intermediates between these states. Second, the EH conformers appear to represent a lower-energy state than the compact HHCs for all polymer sizes studied here. The compact HHC structures seem to be associated with structures that exist in solution or are trapped during the electrospray process. Although it is possible that both conformer types are present in solution, we have not observed strong variations in abundances upon changing solution conditions, as is the case in several other systems.[22,26]

Additional information about the nature of the two types of conformations comes from examining Figure 3, which also shows a comparison of an experimental peak with a calculated distribution for transport of a single conformation through the drift tube.[27] Each peak in the ion mobility distribution is

Compact → Extended Helix Transitions of Polyalanine

J. Phys. Chem. B, Vol. 107, No. 9, 2003 **2115**

substantially broader than calculated peak shapes for transport of a single conformer. The full widths at half-maximum of experimental $[\text{Ala}_n + 3\text{H}]^{3+}$ peaks are 3−5 times broader than values for calculated distributions for transport of a single conformer. At least several related (but not identical) conformations having similar cross sections must be present. The observation of similar broad peaks (although less abundant) at high temperatures requires that these states have similar stabilities. These results are consistent with the range of low-energy structures found in our previous molecular modeling studies.[13]

As a final comment about the experimental distributions, we note that there are no substantial changes in the distributions of conformers in the $[\text{Ala} + \text{H}]^+$ and $[\text{Ala}_n + 2\text{H}]^{2+}$ ions. The distributions of globular conformations previously described for the singly protonated[10−12] and doubly protonated[13] ions appear to be stable even at the highest source temperature.

Discussion

Derivation of Thermochemical Values for Compact → Extended Helix Transitions. A combined analysis of the temperature-dependent datasets allows the thermochemistry associated with the transition state to be determined. Activation energies for the compact → extended helix transitions were obtained by a method that is analogous to one described by Smith and co-workers.[28] For this isomerization reaction, we assume unimolecular kinetics, as described by the equation

$$\frac{-\text{d}[\text{M}_c]}{\text{d}t} = k[\text{M}_c] \qquad (1)$$

where $[\text{M}_c]$ is the concentration of the compact state, t is the reaction time, and k is the rate constant. Upon integration over a fixed time interval, t_1, this relation becomes

$$[\text{M}_c]_1 = [\text{M}_c]_0 e^{-kt_1} \qquad (2)$$

where the subscripts 0 and 1, respectively, denote the concentrations of the compact state before and after the ions are heated in the source capillary. For these studies, $[\text{M}_c]$ is the ratio of integrated signal corresponding to the compact state of a single $[\text{Ala}_n + 3\text{H}]^{3+}$ polymer size to the total integrated signal obtained for that $[\text{Ala}_n + 3\text{H}]^{3+}$ ion. Combining expression 2 with the Arrhenius equation ($k = Ae^{-E_a/RT}$, where A is the preexponential factor, E_a is the activation energy, R is the gas constant, and T is temperature) yields

$$\ln\left(\ln\left(\frac{[\text{M}_c]_0}{[\text{M}_c]_1}\right)\right) = \ln(At_1) + \frac{-E_a}{R}\left(\frac{1}{T}\right) \qquad (3)$$

A plot of $\ln(\ln([\text{M}_c]_0/[\text{M}_c]_1))$ against T^{-1} has a slope of $-E_aR^{-1}$ and an intercept of $\ln(At_1)$.

Reliability of Experimental Thermochemistry. The analysis presented above assumes that (1) all ions are fully desolvated early in the source, (2) solvent-free ions rapidly reach the calibrated source temperature, and (3) ion−solvent interactions in the source do not influence the experimental results. To test these assumptions, additional studies were conducted by varying the capillary length (by as much as a factor of 3). This varies the transmission time through the source, allowing us to examine large effects due to the assumptions that are made. In short, the data obtained under other source conditions are analogous to those reported above; detailed studies using a capillary length of 39.0 cm yielded thermochemical values that are in good

$[\text{Ala}_{36}+3\text{H}]^{3+}$ $i = 36,30,16$
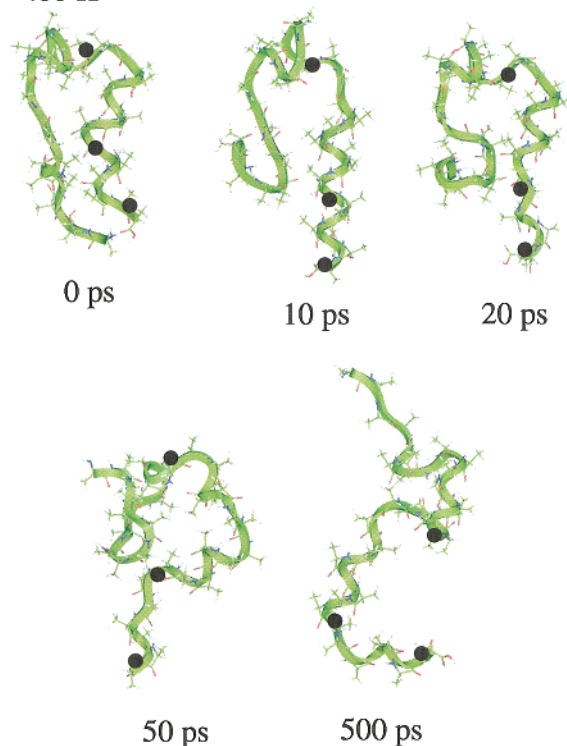400 K

0 ps   10 ps   20 ps

50 ps   500 ps

Figure 7. Model $[\text{Ala}_{36} + 3\text{H}]^{3+}$ conformers obtained by performing 400 K dynamics simulations on a starting geometry identical to the 250-ps conformer shown in Figure 6 in which protons were moved to $i = 36, 30, 16$ locations.

agreement (well within the propagated uncertainties) for all peptide sizes. Thus, under the experimental conditions employed, it appears that ions equilibrate to the source temperature rapidly and are not influenced by solvent.

An additional concern associated with this analysis is that all values of $\ln(\ln([\text{M}_c]_0/[\text{M}_c]_1))$ depend on the accuracy of determining $[\text{M}_c]_0$. Our experience with this system (and the agreement of data for different capillary lengths) indicates that $[\text{M}_c]_0$ is reliable to within $\pm10\%$. In general, as noted by Smith and co-workers, relative activation energies determined by this method should be reliable even if the activation energies on an absolute scale are not as accurate.[28] Because of this, we have reported all of our derived activation energies relative to the value obtained for the shortest polymer length observed.

Relative Activation Energies. Figure 4 shows a representative plot of $\ln(\ln([\text{M}_c]_0/[\text{M}_c]_1))$ against T^{-1} for the $[\text{Ala}_{30} + 3\text{H}]^{3+}$ ions. From a linear fit to the data, we obtain $E_a = 16.7$ kcal·mol^{-1} for the compact → extended helix transition. An analogous procedure was used to determine values of E_a for transitions of the other $[\text{Ala}_n + 3\text{H}]^{3+}$ ($n = 27−39$) ions.[29] Values are reported relative to those derived for $[\text{Ala}_{27} + 3\text{H}]^{3+}$ (the shortest polymer length observed); i.e., the relative E_a for $[\text{Ala}_{27} + 3\text{H}]^{3+}$ was taken to be 0. Relative values for E_a for all polymer sizes are shown in Figure 5. A linear fit to these data indicates that the activation energy for the compact → helix transition increases by 0.9 kcal·mol^{-1}·residue^{-1}. This increase in activation energy with polymer length is consistent with the HHC assignment, as longer polypeptides would be expected to establish more stabilizing interactions between the coil and helical portions.

Proposed Steps in the Compact (HHC) → EH Transition. Molecular modeling studies carried out at elevated temperatures
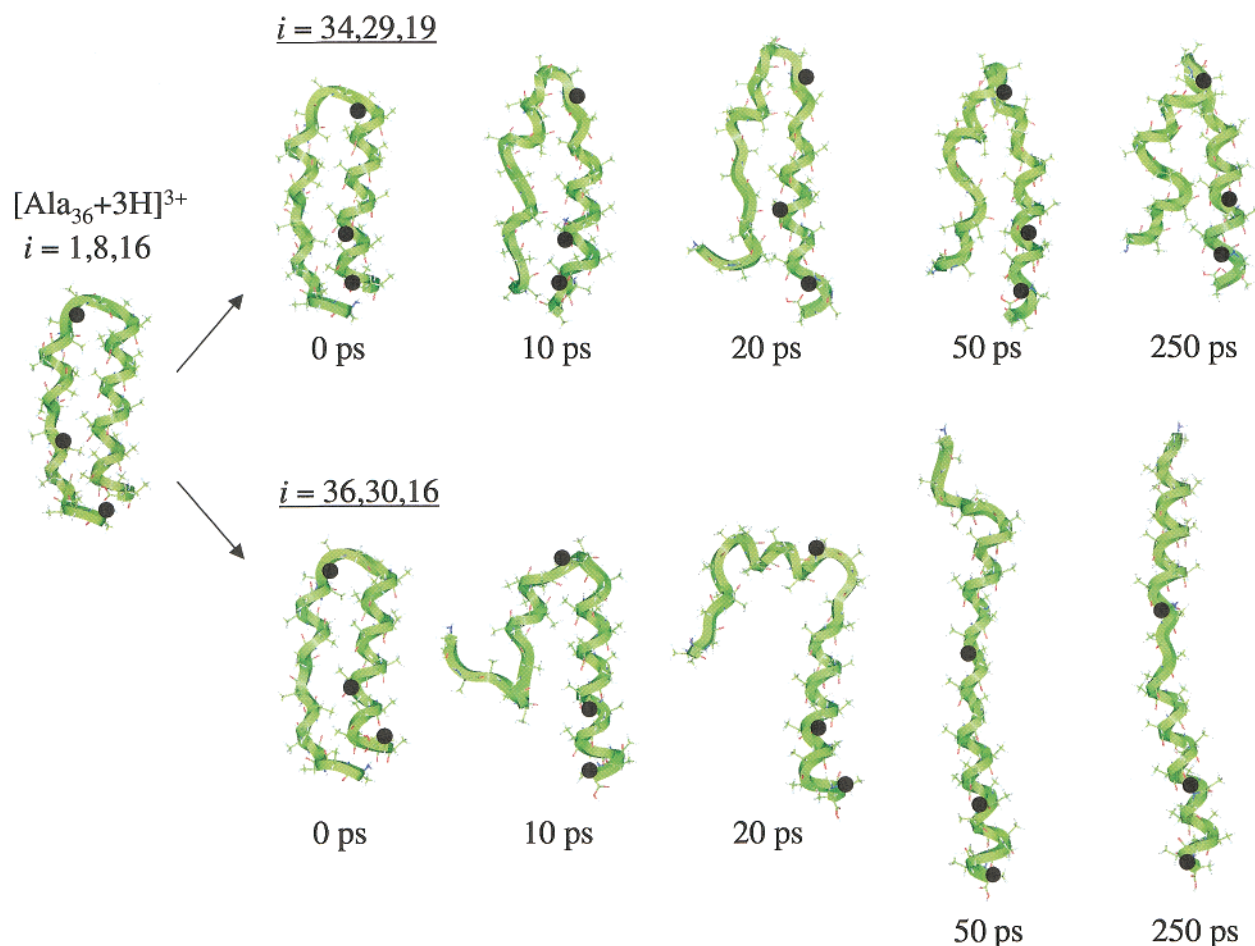
Figure 8. Model $[Ala_{36} + 3H]^{3+}$ conformers obtained from 300 K molecular dynamics simulations by 10, 20, 50, and 250 ps. The starting geometry (0 ps) was the lowest-energy conformer obtained from 300 K dynamics simulations of a 1, 8, 16 charge site assignment (shown at far left). For these simulations, charges were located on the C-terminal helical region of the starting geometry at $i = 36, 30, 16$ (representing transfer of two protons to the C-terminal helical region) and $i = 34, 29, 34$ (representing transfer of all three protons). For each conformer, black filled circles indicate the location of charge sites, and the N- and C-termini are denoted by N and C, respectively.

(400−600 K) on HHC starting geometries [in which the charge assignment is $(\Sigma i)/3 < n/2$] show that, after substantial simulation times, helical turns are lost, and the ions appear to favor more random-like geometries. However, none of the simulations show evidence for the formation of extended geometries. Representative conformers (after simulation times of 50 and 250 ps) from simulations at 400, 500, and 600 K are shown in Figure 6. The inability of this system to generate extended structures (even after long simulations) is expected on the basis of previous studies;[10,11,13] loss of HHC structure leads to random globules.

We have considered two types of mechanisms that would allow extended helices to be formed. In the first mechanism, helical turns and coil contacts are initially disrupted upon heating, and at critical configurations, new less-ordered conformations allow intramolecular proton transfers to occur. Figure 7 shows the results of 400 K dynamics simulations in which two protons are repositioned on a disfigured HHC-like geometry (in this case, charges were repositioned from $i = 1, 8, 16$ to $i = 36, 30, 16$ on the 250-ps structure shown in Figure 6). Many similar simulations (which vary in the details of starting structure and exact positions of charge sites) show similar behavior. Upon redistribution of the protonation sites, substantial progress in generating extended configurations is made. The compact coil rapidly detaches from the helical region; additionally, many of the $i \rightarrow i + 4$ turns that were lost upon heating are reformed upon reorganizing charges to a $(\Sigma i)/3 > n/2$ configuration. This type of mechanism would allow the hinge to open. On the basis

of our previous modeling work, we expect EH conformers to eventually be formed from many different initial conformations. This type of process suggests that an important step in the HHC $\rightarrow$ EH transition involves reaching a structure in which proton transfer can occur and drive the net charge to the C-terminal side of the peptide [i.e., $(\Sigma i)/3 > n/2$].

We have also considered the possibility that intramolecular charge transfer within the HHC conformer initiates the compact state $\rightarrow$ helix transition. This alternative was investigated by initiating the dynamics simulations from HHC structures in which charges were transferred from initial $(\Sigma i)/3 < n/2$ configurations to nearby sites along the C-terminal helical region. Simulations in which as few as one and as many as all three protons were transferred from the N-terminal coil to the C-terminal helical region were carried out. Figure 8 shows example conformers obtained for $[Ala_{36} + 3H]^{3+}$ at various time intervals during 300 K simulations of a HHC geometry in which protons at $i = 1, 8$, and 16 were transferred to $i = 34, 29$, and 19, respectively. Initially, the coil portion of the chain appears to detach from the helical region, adopting a more random (less ordered) structure. At longer times, the N-terminal side of the chain often establishes some $i \rightarrow i + 4$ helical structure. A key step in the formation of extended helices appears to be associated with rearrangement of the hinge portion of the polypeptide such that the system can adopt an extended conformation. Interactions of only a few residues of the coil with the helix (usually through protonation sites) appear to restrict the release of the hinge.

Compact → Extended Helix Transitions of Polyalanine

J. Phys. Chem. B, Vol. 107, No. 9, 2003 **2117**

A similar simulation in which only two protons are transferred from the N- to the C-terminal side is also shown in Figure 8 and provides additional insight into the process of hinge release. In this case, protons at $i = 1$ and 8 on a starting HHC geometry were transferred to $i = 36$ and 30 sites, respectively, on the C-terminal helix; the third proton ($i = 16$) was allowed to remain on the N-terminal side of the hinge. Here, the hinge rapidly opens. By ∼20 ps, the coil portion of the HHC has detached from the helical motif. By 50 ps, the conformer is all but fully extended, and more than 80% of the residues are involved in $i \rightarrow i + 4$ interactions. In this charge site configuration, the rapid release of the hinge appears to be driven by repulsive Coulombic interactions (e.g., upon initial reorganization of the protonation sites, the two protons transferred to the C-terminal helix are in close proximity to the proton that remains on the coil). Simulations performed at 300 or 400 K for similar rearrangements of charge site configurations on other starting HHC geometries (e.g., $i = 1, 6, 12 \rightarrow i = 36, 28, 12$ and $i = 1, 7, 15 \rightarrow i = 36, 27, 15$) exhibit similar general behavior.

Summary and Conclusions

Ion mobility/time-of-flight mass spectrometry techniques have been used to examine structural transitions as a function of temperature for a series of $[\text{Ala}_n + 3\text{H}]^{3+}$ ($n = 27-39$) ions. At room temperature, all of these sizes exhibit two conformations that are stable over the $10-40$-ms time scales of these experiments: a low-mobility family of extended helical structures and a higher-mobility family of hinged helix-coil geometries.[13] At high temperatures, the extended helical state is favored for all polymer sizes. Relative activation energies for the compact → extended helix transitions increase by ∼0.9 kcal·mol^{-1}·residue^{-1} from $n = 27$ to $n = 39$. Possible mechanisms for the compact (hinged helix-coil) → extended helix transition have been considered. It appears that intramolecular proton transfer and separation of the coil and helical regions within the compact state are key steps in forming extended helices.

References and Notes

(1) Aurora, R.; Creamer, T. P.; Srinivasan, R.; Rose, G. D. *J. Biol. Chem.* **1997**, *272*, 1413.

(2) Shea, J.-E.; Onuchic, J. N.; Brooks, C. L., III. *J. Chem. Phys.* **2000**, *113*, 7663.

(3) Padmanabhan, S.; Marqusee, S.; Ridgeway, T.; Laue, T. M.; Baldwin, R. L. *Nature* **1990**, *344*, 268. Chakrabartty, A.; Schellman, J. A.; Baldwin, R. L. *Nature* **1991**, *351*, 586.

(4) Millhauser, G. L.; Stenland, C. J.; Hanson, P.; Bolin, K. A.; van de Ven, F. J. M. *J. Mol. Biol.* **1997**, *267*, 963.

(5) Long, H. W.; Tycko, R. *J. Am. Chem. Soc.* **1998**, *120*, 7039.

(6) Ramamoorthy, A.; Lee, D.-K. *J. Phys. Chem. B* **1999**, *103*, 271.

(7) Ingwall, R. T.; Scheraga, H. A.; Lotan, N.; Berger, A.; Katchalski, E. *Biopolymers* **1968**, *6*, 331. Vila, J.; Williams, R. L.; Grant, J. A.; Wojcik, J.; Scheraga, H. A. *Proc. Natl. Acad. Sci. U.S.A.* **1992**, *89*, 7821. Kemp, D. S.; Boyd, J. G.; Muendel, C. C. *Nature* **1991**, *352*, 451. Renold, P.; Tsang, K. Y.; Shimizu, L. S.; Kemp, D. S. *J. Am. Chem. Soc.* **1996**, *118*, 12234. Groebke, K.; Renold, P.; Tsang, K. Y.; Allen, T. J.; McClure, K. F.; Kemp, D. S. *Proc. Natl. Acad. Sci. U.S.A.* **1996**, *93*, 4025. Spek, E. J.; Olson, C. A.; Shi, Z.; Kallenbach, N. R. *J. Am. Chem. Soc.* **1999**; *121*, 5571.

(8) Fenn, J. B.; Mann, M.; Meng, C. K.; Wong, S. F.; Whitehouse, C. M. *Science* **1989**, *246*, 64.

(9) For examples of structural studies of peptides and protein ions in the gas phase, see: (a) Wood, T. D.; Chorush, R. A.; Wampler, F. M.; Little, D. P.; O'Connor, P. B.; McLafferty, F. W. *Proc. Natl. Acad. Sci. U.S.A.* **1995**, *92*, 2451. (b) Covey, T. R.; Douglas, D. J. *J. Am. Soc. Mass Spectrom.* **1993**, *4*, 616. (c) Ogorzalek Loo, R. R.; Smith, R. D. *J. Am. Soc. Mass Spectrom.* **1994**, *5*, 207. (d) Wyttenbach, T.; von Helden, G.; Bowers, M. T. *J. Am. Chem. Soc.* **1996**, *118*, 8355. (e) Clemmer, D. E.; Hudgins, R. R.; Jarrold, M. F. *J. Am. Chem.* Soc. **1995**, *117*, 10141. (f) Schnier, P. F.; Gross, D. S.; Williams, E. R. *J. Am. Chem. Soc.* **1995**, *117*, 6747. (g) McLuckey, S. A.; Goeringer, D. E. *Anal. Chem.* **1995**, *67*, 2493. (h) Kaltashov, I. A.; Fenselau, C. C. *J. Am. Chem. Soc*. **1995**, *117*, 9906. (i) Cassady, C. J.; Carr, S. R. *J. Mass Spectrom.* **1996**, *93*, 3143. (j) Sullivan, P. A.; Axelsson, J.; Altmann, S.; Quist*,* A. P.; Sunqvist, B. U. R.; Reimann, C. T. *J. Am. Soc. Mass Spectrom.* **1996**, *7*, 329. (k) Valentine, S. J.; Anderson, J.; Ellington, A. E.; Clemmer, D. E. *J. Phys. Chem. B* **1997**, *101*, 3891.

(10) Hudgins, R. R.; Mao, Y.; Ratner, M. A.; Jarrold, M. F. *Biophys. J.* **1999**, *76*, 1591.

(11) Samuelson, S.; Martyna, G. J. *J. Phys. Chem. B* **1999**, *103*, 1752.

(12) Hudgins, R. R.; Ratner, M. A.; Jarrold, M. F. *J. Am. Chem. Soc.* **1998**, *120*, 12974.

(13) Counterman, A. E.; Clemmer, D. E. *J. Am. Chem. Soc.* **2001**, *123*, 1490.

(14) Pauling, L.; Corey, R. B.; Branson, H. R. *Proc. Natl. Acad. Sci. U.S.A.* **1951**, *37*, 205. Poland, D.; Scheraga, H. A. *Theory of Helix-Coil Transitions in Biopolymers*; Academic Press: New York, 1970. Serrano, L. *Adv. Protein Chem.* **2000**, *53*, 50. Son, H. S.; Hong, B. H.; Lee, C.-W.; Yun, S.; Kim, K. S. *J. Am. Chem. Soc.* **2001**, *123*, 514.

(15) Gidden, J.; Wyttenbach, T.; Batka, J. J.; Weis, P.; Jackson, A. T.; Scrivens, J. H.; Bowers, M. T. *J. Am. Chem. Soc.* **1999**, *1221*, 1421. Gidden, J.; Bushnell, J. E.; Bowers, M. T. *J. Am. Chem. Soc.* **2001**, *123*, 5610.

(16) Shelimov, K. B.; Jarrold, M. F. *J. Am. Chem. Soc.* **1997**, *119*, 2987. Kinnear, B. S.; Hartings, M. R.; Jarrold, M. F. *J. Am. Chem. Soc.* **2001**, *123*, 5660.

(17) Hagen, D. F. *Anal. Chem.* **1979**, *51*, 870. Hill, H. H.; Siems, W. F.; St. Louis, R. H.; McMinn, D. G. *Anal. Chem.* **1990**, *62*, 1201A.

(18) For recent reviews of ion mobility studies of biomolecules, see: Clemmer, D. E.; Jarrold, M. F. *J. Mass Spectrom.* **1997**, *32*, 577. Hoaglund Hyzer, C. S.; Counterman, A. E.; Clemmer, D. E. *Chem. Rev.* **1999**, *99*, 3037.

(19) Hoaglund, C. S.; Liu, Y.; Pagel, M.; Ellington, A. D.; Clemmer, D. E. *J. Am. Chem. Soc.* **1997**, *119*, 9051.

(20) Counterman, A. E.; Clemmer, D. E. *J. Am. Chem. Soc.* **1999**, *121*, 4031.

(21) Hoaglund, C. S.; Valentine, S. J.; Sporleder, C. R.; Reilly, J. P.; Clemmer, D. E. *Anal. Chem.* **1998**, *70*, 2236. Henderson, S. C.; Valentine, S. J.; Counterman, A. E.; Clemmer, D. E. *Anal. Chem.* **1999**, *71*, 291.

(22) Li, J.; Taraszka, J. A.; Counterman, A. E.; Clemmer, D. E. *Int. J. Mass Spectrom. Ion Processes* **1999**, *185/186/187*, 37.

(23) Rockwood, A. L.; Busman, M.; Udseth, H. R.; Smith, R. D. *Rapid Commun. Mass Spectrom.* **1991**, *5*, 582.

(24) Penn, S. G.; He, F.; Green, M. K.; Lebrilla, C. B. *J. Am. Soc. Mass Spectrom.* **1997**, *8*, 244.

(25) von Helden, G.; Hsu, M.-T.; Kemper, P. R.; Bowers, M. T. *J. Chem. Phys.* **1991**, *95*, 3835. Jarrold, M. F.; Constant, V. A. *Phys. Rev. Lett.* **1991**, *67*, 2994. Clemmer, D. E.; Hudgins, R. R.; Jarrold, M. F. *J. Am. Chem. Soc.* **1995**, *117*, 10141.

(26) Hudgins, R. R.; Woenckhaus, J.; Jarrold, M. F. *Int. J. Mass Spectrom. Ion Processes* **1997**, *165/166*, 497.

(27) The expression for transport of a single conformer type across the drift tube is given by

$$\Phi(t) = \int \frac{C}{(Dt)^{1/2}} (v_D + L/t) \left[1 - \exp\left(\frac{-r_o^2}{4Dt}\right) \right] \exp\left[\frac{-(L - v_D t)^2}{4Dt}\right] P(t_p) \, dt_p$$

where $\Phi(t)$ is the intensity of ions passing through the exit aperture as a function of time, C is a constant, D is the diffusion constant, t is the time, r_o is the drift tube entrance aperture radius, v_D is the measured drift velocity, L is the drift tube length, and $P(t_p) \, dt_p$ is the distribution function for the pulse of ions entering the drift tube. For a further discussion, see: Mason, E. A.; McDaniel, E. W. *Transport Properties of Ions in Gases*; Wiley: New York, 1988.

(28) Busman, M.; Rockwood, A. L.; Smith, R. D. *J. Phys. Chem.* **1992**, *96*, 2397.

(29) Values of E_a were not derived for $n < 27$ and $n = 40$ because the fraction of compact state ($n < 27$) or total ion population ($n = 40$) present at elevated temperatures was very small (within the limits of the signal-to-noise ratio).